PCCP

Cite this: *Phys. Chem. Chem. Phys.*, 2011, **13**, 16800–16810

www.rsc.org/pccp

PAPER

Adsorption energetics of CO on supported Pd nanoparticles as a function of particle size by single crystal microcalorimetry

J. M. Flores-Camacho,[a] J.-H. Fischer-Wolfarth,[a] M. Peter,[a] C. T. Campbell,[b] S. Schauermann*[a] and H.-J. Freund[a]

Received 24th May 2011, Accepted 5th August 2011
DOI: 10.1039/c1cp21677e

The heat of adsorption and sticking probability of CO on well-defined Pd nanoparticles were measured as a function of particle size using single crystal adsorption microcalorimetry. Pd particles of different average sizes ranging from 120 to 4900 atoms per particle (or from 1.8 to 8 nm) and Pd(111) were used that were supported on a model *in situ* grown Fe_3O_4/Pt(111) oxide film. To precisely quantify the adsorption energies, the reflectivities of the investigated model surfaces were measured as a function of the thickness of the Fe_3O_4 oxide layer and the amount of deposited Pd. A substantial decrease of the binding energy of CO was found with decreasing particle size. Initial heat of adsorption obtained on the virtually adsorbate-free surface was observed to be reduced by about 20–40 kJ mol^{-1} on the smallest 1.8 nm sized Pd particles as compared to the larger Pd clusters and the extended Pd(111) single crystal surface. This effect is discussed in terms of the size-dependent properties of the Pd nanoparticles. The CO adsorption kinetics indicates a strong enhancement of the adsorbate flux onto the metal particles due to a capture zone effect, which involves trapping of adsorbates on the support and diffusion to metal clusters. The CO adsorption rate was found to be enhanced by a factor of $\sim$8 for the smallest 1.8 nm sized particles and by $\sim$1.4 for the particles of 7–8 nm size.

Introduction

Nanoparticles of transition metals supported on the oxide surfaces form a basis for a large variety of practically important catalytic materials. Their structural properties, *e.g.* the particle size, are believed to strongly affect or even control the chemical activity of a catalyst.[1–7] Generally, the overall activity of any catalytic surface depends on the two classes of its properties: on the intrinsic activity of the metal to catalyze the desired reaction pathway and on the ability of the surface to efficiently bind the reactants, stabilize the desired reaction intermediates and effectively release the products. The latter group of the properties is determined by the bond strength of the adsorbed surface species and by the relative thermodynamic stabilities of the reaction intermediates. For the controlled molecular design of new catalytic materials, a detailed knowledge on the energetics of the adsorbate–surface interaction is required, which provides a basis for fundamental understanding of how the surface binds the reactants and guides them through various elementary steps to the products. For the practically-important nano-structured materials, such fundamental information on the correlation between the gas–surface binding energy and the exact nature of an adsorption site as well as the size of the metal nanoparticles is not available. Previously, such correlations were addressed by adsorption calorimetry by Vannice *et al.* on powdered supported Pt, Pd and Ni catalysts.[8] However, studies of such powdered materials produced by wet chemical preparation can suffer from impurities and inhomogeneities of the support, resulting in a broad particle size, structure or even composition distribution. The vast complexity of such materials and possible contaminations introduced during wet chemical preparation hamper detailed understanding of the structure of the metal nanoparticles and the nature of the surface sites interacting with the adsorbates.

To overcome the above-mentioned problems, we adopt here a model catalyst approach where clean and well-defined metal nanoparticles are prepared on single-crystalline oxide films grown on metal single crystals under the pristine conditions of ultrahigh vacuum (UHV).[2,4,9–14] The use of such model surfaces allows us to controllably vary the degree of complexity of supported catalysts and enables a detailed characterization of their surface structure by a variety of surface science methods without losing the catalytically important structural properties inherent to dispersed supported catalysts. Previously, the adsorption energetics of several gases were studied as a function of particle size by temperature programmed desorption (TPD) for clean and well-defined metal nanoparticles on

[a] *Fritz-Haber-Institut der Max-Planck-Gesellschaft, Faradayweg 4-6, 14195 Berlin, Germany. E-mail: schauermann@fhi-berlin.mpg.de*
[b] *Department of Chemistry, Box 351700, University of Washington, Seattle, WA 98195-1700, USA*

single crystalline oxide surfaces (see *e.g.* ref. 3, 15 and 16). However, those studies generally must assume a preexponential factor for desorption to get the activation energy for desorption, and must further assume that there is no activation barrier for adsorption to convert the activation energy for desorption into adsorption energy. Also, the initial particle size distribution can change during the heating required for such TPD studies.

In order to surmount these restrictions, we have developed the capability to *directly* measure heats of adsorption by a single crystal adsorption calorimeter (SCAC) on model catalysts consisting of clean and well-defined metal nanoparticles grown on single-crystalline oxide surfaces under UHV,[17] which provides much more definitive understanding of the relationship between adsorbate energetics and catalyst nanostructure. We report here calorimetric measurements of the adsorption energy of CO molecules as a detailed function of Pd particle size for model Pd/Fe_3O_4 catalysts consisting of well-defined Pd nanoparticles supported on clean $Fe_3O_4(111)$ single-crystalline surfaces, grown as thin films on a Pt(111) substrate in an ultrahigh vacuum. The adsorption energies were systematically measured as a function of CO surface coverage and the size of Pd nanoclusters (independently characterized by scanning tunneling microscopy in ref. 18). Previous attempts to address the particle-size effects on the CO chemisorption energy by temperature-programmed desorption[15] and isothermal modulated molecular beam studies[11,19] provided contradictory results: whereas the TPD studies found a decrease of the adsorption energy by about 10 kJ mol^{-1} on the 2.5 nm-sized Pd particles as compared to the extended single crystal surfaces, the molecular beam experiments predicted a pronounced increase of the adsorption energy by about 35 kJ mol^{-1} on the particles smaller than 1.5 nm. With the direct SCAC measurement of the CO adsorption heats we obtained a pronounced decrease of the adsorption energy with decreasing particle size and resolved with this a long-standing controversy. A preliminary report of some of these results has appeared elsewhere.[20]

Experimental procedure

The adsorption experiments were performed at the Fritz-Haber-Institute (Berlin) in a UHV single crystal adsorption calorimetry apparatus described in detail elsewhere.[17] Briefly, the apparatus consists of two independent UHV chambers, separated by a gate valve, with typical base pressure 2×10^{-10} mbar. An effusive doubly differentially pumped multichannel array source was employed to produce a CO (Linde, purity 4.7) beam at the intensity of 9.24×10^{13} molecules cm^{-2} s^{-1} (3.3×10^{-7} mbar on the sample surface). The beam was cut into pulses of 266 ms length by a remote-controlled chopper, after that the gas impinged on a sample prepared on an ultrathin (1 μm) single crystal (Pd(111) or Pt(111)). The beam spot on the sample surface had a circular shape with the diameter of 4 mm. During the gas exposure, a fraction of the molecule adsorbs on the surface, producing a heat input, which causes a small (~10–20 mK) transient temperature rise in the crystal. This small change in the temperature of the sample was measured by a heat detector, consisting of a 9 μm-thick β-polyvinylidene fluoride (β-PVDF) pyroelectric ribbon coated with Au on both sides, which produces a transient voltage signal proportional to the temperature change. The energy calibration was performed by applying pulses of laser light (HeNe, Linos, wavelength 632.8 nm, 5 mW), which passes through the same path as the molecular beam and is chopped in a way identical to the molecular flux. Simultaneously, the fraction of the molecules adsorbed in a single beam pulse (*i.e.*, the sticking coefficient) was measured by the modified King–Wells method[21] with a quadrupole mass spectrometer (QMS Hiden, HAL 301/3F) in a non-line-of-sight geometry.

The absolute laser power was measured by an *in situ* photodiode (Thorlabs, calibrated: 472.2 μW V^{-1}) installed in the UHV chamber. The reflectivity of the sample was determined by the use of a newly developed *in situ* setup for reflectivity measurements with a continuous-wave He–Ne laser (λ = 632.8 nm), which is described in detail elsewhere.[17] The reflectivity was measured on the samples prepared on the 1 mm-thick crystals, prepared in the same way as the 1 μm-thin samples in order to guarantee the macroscopic flatness of the surfaces.

The Pd(111) single crystal, which is used as a reference for CO adsorption on extended surfaces, was cleaned by repeated cycles of sputtering with 800 eV Ar ions, oxidation at 700 K and annealing at 1000 K. The $Pd/Fe_3O_4/Pt(111)$ model catalyst was prepared by growing a thin (~50 Å) $Fe_3O_4(111)$ film on a Pt(111) single crystal by repeated cycles of Fe (>99.99%, Goodfellow) physical vapor deposition at a substrate temperature of ~120 K and subsequent oxidation at 875 K (see ref. 18, 22–25 for details). The cleanliness and the quality of the oxide film was checked by AES and LEED. Pd particles were grown *in situ* by physical vapor deposition from a Pd rod (>99.9%, Goodfellow) using a commercial evaporator (Focus, EFM 3) with a deposition rate of 0.3 Å min^{-1} (2.1×10^{14} atoms cm^{-2} min^{-1}). During metal evaporation, the single crystal sample was held at 115 K, and biased to +800 V to avoid formation of defects by metal ions. The mean diameter of the resulting Pd particles was controlled by the amount of deposited Pd, which was varied from 2.1×10^{14} to 4.9×10^{15} atoms cm^{-2} using five nominal deposition thickness values (0.3, 0.6, 1.5, 4.0, and 7.0 Å, where 1 Å corresponds to 7×10^{14} atoms cm^{-2} assuming the bulk density of Pd). Directly after Pd deposition, the sample was annealed to 600 K and cooled, and a microcalorimetric measurement of CO adsorption heats was performed after the sample reached thermal equilibrium near room temperature with the pyroelectric detector. The evaporation rates of Fe and Pd were calibrated by a quartz-crystal microbalance (QCM, Sigma instruments).

Results and discussion

1. Structure of $Pd/Fe_3O_4/Pt(111)$ model supported catalysts

To study the CO adsorption energies as a function of particle size, a series of the $Pd/Fe_3O_4/Pt(111)$ model supported catalysts with five different nominal Pd coverages was prepared. Fig. 1 shows scanning tunneling microscopy (STM)

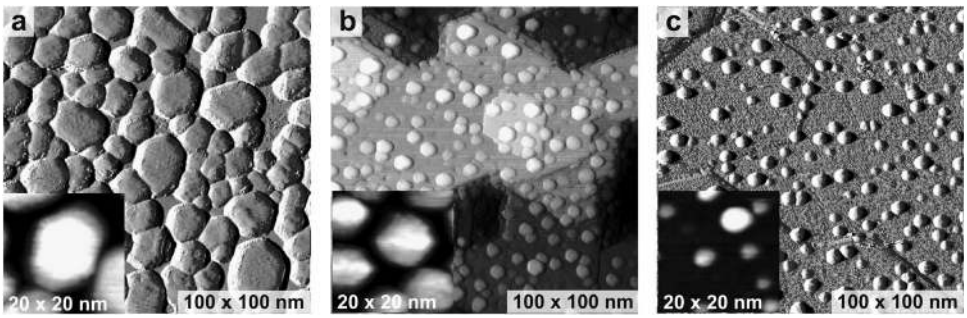

Fig. 1 STM images (100 × 100 nm) of Pd particles on Fe_3O_4/Pt(111) for different Pd nominal thicknesses: (a) 7 Å, (b) 4 Å, and (c) 0.3 Å, from ref. 24.

Table 1 Structural data of the Pd/Fe_3O_4 model catalysts as determined from STM (see Fig. 1), and the measured number of CO molecules adsorbed per particle in the first CO gas pulse during calorimetry

Nominal thickness of deposited Pd layer	0.3 Å	4.0 Å	7.0 Å
Nominal Pd coverage/atoms cm^{-2}	2.1×10^{14}	2.8×10^{15}	4.9×10^{15}
Pd particle density from STM/cm^{-2}	1.7×10^{12}	3.8×10^{12}	1.0×10^{12}
Average number of Pd atoms per particle	~120	~740	~4900
Average Pd particle diameter/nm	1.8	4	8
Estimated number of surface Pd atoms per particle	~65	~240	~870
Number of CO molecules per Pd island adsorbed in the first MB pulse	~4	~3	~14

images for three surfaces with Pd thicknesses of 0.3, 4 and 7 Å (from ref. 24). Table 1 summarizes the structural data derived from the STM images. The average number of Pd atoms per particle was estimated by dividing the Pd coverage by the Pd particle density. Additionally, the average number of the surface Pd atoms per particle was estimated from these structural data assuming a hemispherical particle shape to first estimate the Pd particle radius, and then assuming the same number of Pd surface atoms per unit area as on the Pd(111) surface (these numbers are reported in Table 1 as number of Pd atoms per cm^2).

At the highest investigated Pd coverage (7 Å, Fig. 1a), nucleation of the Pd particles occurs in a well-distributed fashion over the Fe_3O_4 terraces resulting in formation of ~10^{12} Pd particles per cm^2. The inset shows a close-up of an individual particle, which has a hexagonal shape with a rather flat top facet. This indicates that the crystalline aggregates are formed, growing in (111) orientation, and their sides are terminated either with (111) or (100) facets. The average number of Pd atoms per particle is estimated to be about ~4900 here. For the nominal deposition thickness of 4 Å, the island density grows by about a factor of 4 resulting in formation of smaller particles (~740 Pd atoms per island, Fig. 1b) that retain a hexagonal form and a high degree of crystallinity. At the lowest investigated Pd coverage (0.3 Å, Fig. 1c), the shape of the particles appears round. However, it should be kept in mind that due to convolution with the tip shape, the precise identification of the particle shape and size is difficult in the small particle size limit.[2] The average number of Pd atoms per particle is estimated to be about 120, corresponding to the particle size of ~1.8 nm.

2. Optical reflectivity of Pd/Fe_3O_4/Pt(111) surfaces

The reflectivity of the model catalyst surfaces was determined both on pristine Fe_3O_4/Pt(111) layers after the different stages of oxide film preparation and on the oxide layer containing Pd nanoclusters.

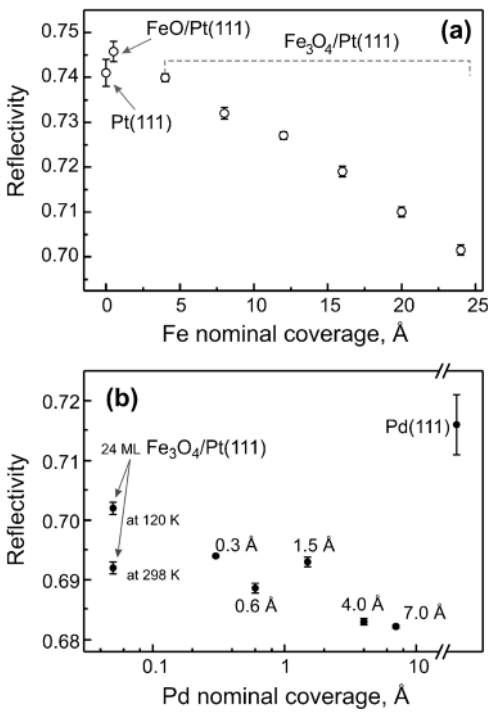

Fig. 2 Optical reflectivity measurements at the He–Ne laser wavelength of 632.8 nm at normal incidence, as used for calorimeter calibration, for: (a) Pt(111), FeO/Pt(111) and Fe_3O_4(111)/Pt(111) after successive cycles of preparation plotted as a function of the thickness of the iron layer (Å) deposited prior to oxidation (see text). The reflectivity is measured at 120 K directly after oxidation. (b) Fe_3O_4/Pt(111) film (obtained after consecutive deposition and oxidation of 24 Å of Fe) covered with different amounts of Pd nanoparticles, plotted here as a function of their Pd nominal coverage (measured at 298 K).

Fig. 2a shows the reflectivity values obtained at a photon energy of 1.96 eV (λ = 632.8 nm) on the pristine Pt(111) crystal, on the same crystal after preparation of the closed FeO

monolayer film and after each of the six successive cycles of Fe_3O_4 preparation. The reflectivity measurements were carried out at 120 K. A clean Pt(111) surface shows a 74.1 ± 0.3% reflectivity, which remains nearly the same within the experimental error after formation of the FeO monolayer (74.6 ± 0.2%). On the following stages of preparation, formation of Fe_3O_4 layers significantly affects the reflectivity leading to a decrease from 74.6 ± 0.2% on the FeO layer to 70.2 ± 0.1% after deposition of 24 Å of iron, resulting in the formation of a thick Fe_3O_4 film. The deposited Fe thickness of 24 Å, once oxidized, corresponds to 1.1×10^{-8} moles Fe_3O_4 per cm^2, which at its bulk density corresponds to an effective thickness of 50 Å of Fe_3O_4.

The decrease in the reflectivity of the resulting Fe_3O_4 film ΔR scales linearly with the amount of deposited iron: $\Delta R = (-01.9 \pm 0.06\%) \times d_{Fe}$, where d_{Fe} (Å) is the thickness of the iron layer deposited prior to oxidation (note that d_{Fe} is not the thickness of the resulting Fe_3O_4 film). 1 Å of deposited iron corresponds to deposition of 8.5×10^{14} Fe atoms per cm^2 assuming the density of bulk iron.

Note that the reflectivity changes as a function of surface temperature. The reflectivity of pristine Pt(111) decreases from 74.1 ± 0.3% to 73.1 ± 0.1% when the temperature increases from 120 K to 298 K. This reflectivity decrease is related to a change of the dielectric function with increasing temperature.[26] The reflectivity of Pt(111) determined at 298 K coincides within 3% with most of the published data on the reflectivity of Pt. A reflectivity value of 75% was reported by Yu *et al.* for an evaporated Pt film,[27] 71.5 ± 0.5% by King *et al.* for Pt(111)[28] and 76% by Campbell *et al.* for Pt(111).[29] A substantially lower reflectivity of 67% was measured on a polycrystalline Pt sample by Weaver.[30] The reflectivity of the final Fe_3O_4/Pt(111) obtained after deposition and oxidation of 24 Å of Fe amounts to 70.2% ± 0.1% at 120 K and 69.2 ± 0.1% at 289 K.

The reflectivities of Pd(111) and five Pd/Fe_3O_4/Pt(111) samples with different amounts of deposited Pd were studied at room temperature. Fig. 2b shows the obtained values plotted as a function of Pd deposition thickness along with the reflectivity for the Pd(111) surface. For Pd(111), the measured value of 71.6 ± 0.5% lies in the range between 70.6% and 72.9% of the previously obtained reflectivity values.[31–34] For Pd nanoparticles supported on the Fe_3O_4 film, a decreasing reflectivity was observed with increasing amount of deposited Pd. This behavior is expected from the increasing absorption of light as a function of incrementing particle size.[35] To estimate a possible contribution of scattering to the reflectivity changes with increasing particles size, we calculated the absorption and scattering efficiencies of the free-standing single Pd particle using Mie theory.[36] In the scope of this theory, the absorption efficiency exceeds the scattering efficiency by ~300-fold for the 8 nm sized clusters and by $\sim 2.5 \times 10^4$ for the 1.8-sized Pd particles. From this estimate it can be assumed that the decreasing reflectivity of the Pd/Fe_3O_4/Pt(111) surfaces with increasing particles size results mainly from the increasing absorption of light by the metal particles. For the three lowest Pd deposition thicknesses, 0.3, 0.6 and 1.5 Å, the reflectivity values coincide within less than 1% of the bare Fe_3O_4/Pt(111) support at room temperature. For the larger deposition thicknesses, the trend to lower reflectivities (68.3% and 68.2% for 4 and 7 Å deposited Pd, correspondingly) is more pronounced. It should be mentioned that the final reflectivity might be affected by fluctuations of the evaporation rate of Fe resulting in a slightly different thickness of the underlying Fe_3O_4 layer. To minimize the impact of this irreproducibility on the measured adsorption energy values below (whose calibration is sensitive to sample reflectivity), the adsorption energy measurements reported below were carried out on several—typically four to six—newly prepared samples and averaged.

3. Combined energy and sticking coefficient measurement: CO adsorption on supported Pd nanoparticles

A typical complete calorimetric data set is shown in Fig. 3. Fig. 3a displays the response of the pyroelectric ribbon plotted as a function of time due to the adsorption of CO gas pulses onto Pd nanoparticles (deposition thickness 7 Å) supported on Fe_3O_4(111)/Pt(111) films at 300 K. The applied molecular beam flux amounts to 9.3×10^{13} CO molecules cm^{-2} s^{-1}, which in combination with the pulse length of 266 ms results in 2.5×10^{13} CO molecules cm^{-2} supplied to the surface per molecular beam pulse. The energy released per CO pulse is presented as a function of the pulse number in Fig. 3b. Fig. 3c shows the time evolution of the corresponding QMS signal for CO gas (28 amu), recorded simultaneously with the calorimetric measurement. This trace is used to calculate the sticking probabilities of CO *via* the King–Wells method,[21] which are displayed in Fig. 3d as a function of CO pulse number.

Note that in a microcalorimetry experiment carried out under conditions where the adsorbate can desorb in the ~2 s time between pulses, which is the case at high coverages in Fig. 3, the system always reaches a steady-state situation at quasi-saturation. In this regime, there is a constant non-zero sticking probability and constant adsorption heat even after saturation of the surface at high exposures. This effect is a consequence of the fact that the CO saturation coverage depends on the CO pressure in the gas phase:[37,38] it is higher while the surface is exposed to the molecular beam and decreases after the interruption of the beam toward the value inherent to UHV conditions. As a result, a part of the molecules desorbs between molecular beam pulses and overall a quasi saturation regime is reached, in which the adsorption during a gas pulse exactly balances the desorption between gas pulses. This behavior leads to an apparent infinite uptake of gas onto the surface in a quasi-saturation regime. Similar behavior was previously observed in the microcalorimetric studies on CO adsorption carried out on the Pd, Pt and Ni single crystal surfaces[39] and cyclohexene on Pt(111).[40] To quantitatively treat this phenomenon, Campbell *et al.* introduced two types of sticking probabilities for calorimetry experiments:[40] the long-time sticking probability, which is defined as the probability that molecules in a gas pulse stick on the surface until the next pulse arrives 2 s later, and the short-time sticking probability, which is defined as the probability that molecules in a gas pulse stick on the surface until the end of that gas pulse, which is the time period used to measure the heat signal. In Campbell's work, the long-time

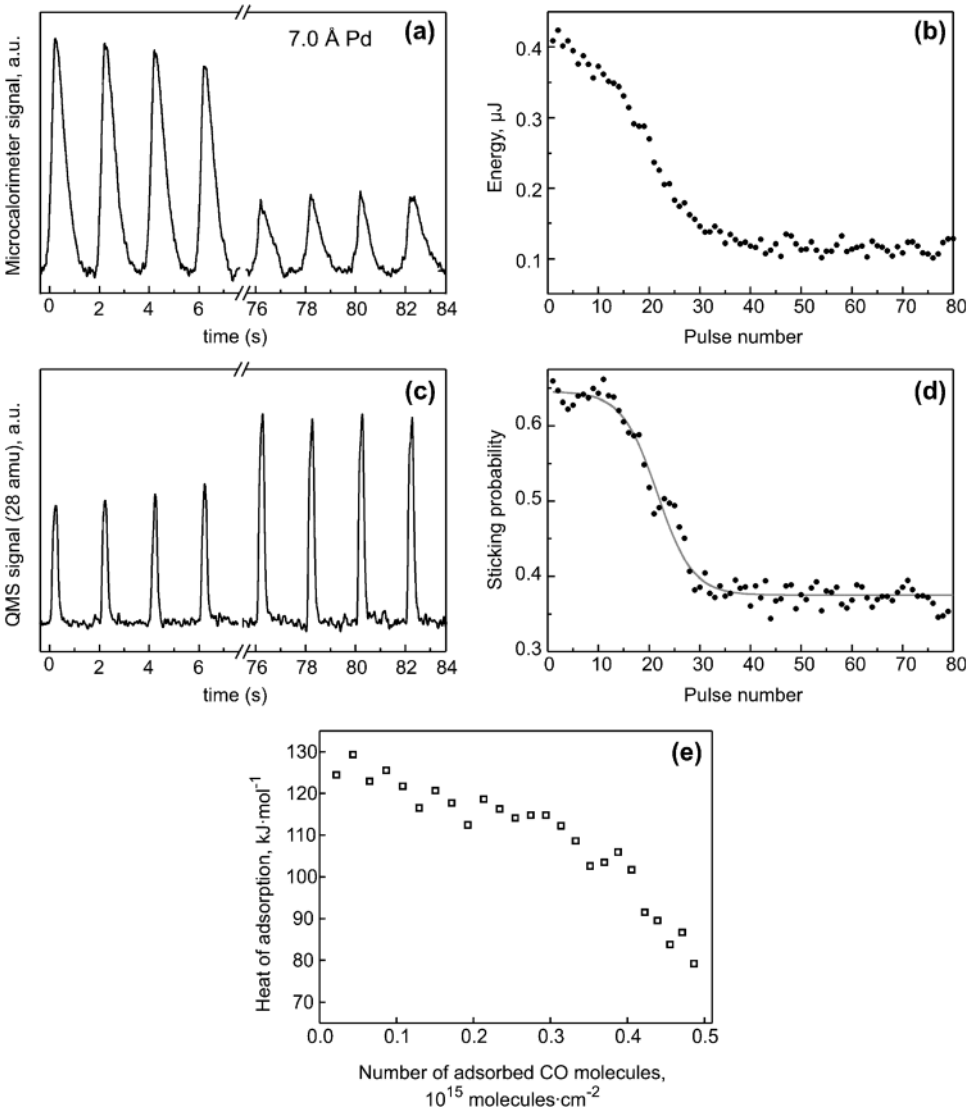

Fig. 3 A typical dataset obtained upon adsorption of CO on 7 Å $Pd/Fe_3O_4/Pt(111)$ at 300 K (with the effective thickness of the oxide layer ~50 Å): (a) the pyroelectric detector response from a train of CO pulses (CO flux: 2.6×10^{13} CO molecules cm^{-2} per pulse or 0.017 ML per pulse); (b) the energy released per CO pulse plotted as a function of pulse number; (c) time evolution of the QMS signal at 28 amu used for calculation of the sticking probability; (d) resulting sticking probability plotted as a function of pulse number; (e) differential heats of adsorption plotted as a function of number of adsorbed CO molecules.

sticking probabilities were used to calculate the coverage at the start of the next pulse, and the short-time sticking probabilities were utilized for calculation of the adsorption energies *per mole adsorbed*. When the quasi-equilibrium is reached, the long-term sticking probability goes to zero (*i.e.*, the coverage at the start of each new pulse is the same) but the short-term sticking probability may remain very high. When there is no desorption between pulses, both sticking coefficients must be the same.

In the present work, only short-time sticking coefficients were measured. As seen in Fig. 3d, the initial short-time sticking probability on the clean sample is 0.64 ± 0.01 at 300 K and decreases to a constant value of 0.38 ± 0.01 after ~32 CO pulses in quasi-saturation. The latter sticking coefficient corresponds to adsorption during the pulse and desorption between the pulses of about 0.01 CO molecules per surface Pd atom, which is small as compared to the CO saturation coverage of 0.5 CO molecules per surface Pd atom at 300 K (see below). The short-time sticking coefficient and flux allow us to calculate the absolute number of CO molecules that were adsorbed on the surface during each pulse. Assuming that no significant amounts of CO desorb between pulses *prior to the quasi saturation regime is reached*, the increase of the total CO surface coverage as a function of the pulse number can be calculated by integrating the sticking coefficient and multiplying the obtained number with the CO flux.[21] However, it should be kept in mind that the use of the short-time sticking coefficients can generally lead to over-estimation of the CO surface coverage, due to long-time desorption of CO between pulses. For the coverages reported in the present study, this is not an important problem, since we truncated the coverage measurements just before saturation,

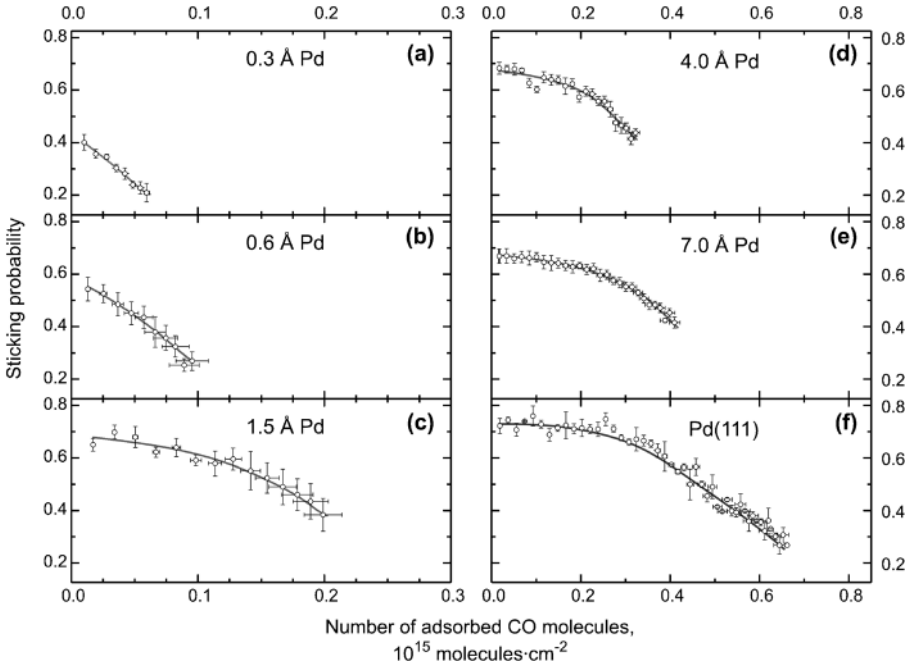

Fig. 4 Sticking probability plotted as a function of number of adsorbed CO molecules at 300 K for Pd(111) and for Pd nanoparticles of different sizes (the Pd nominal coverages are indicated). The data are shown as an average of four to six independent measurements on freshly prepared surfaces. The error bars correspond to the error of the mean.

where the short-time sticking probability and the long-time sticking probability are still very similar. We verified that the use of the short-time sticking coefficients for CO adsorption on Pd particles and Pd(111) gives the same CO coverages (within 0.2% for Pd(111) and ~6% on Pd particles) as the true values measured with a continuously running molecular beam in the coverage regime reported here.

As shown in Fig. 3b, at the beginning of the exposure, the initial adsorption energy on the clean Pd clusters is high (415 ± 7 nJ per pulse), which decreases with increasing CO exposure until it reaches the quasi-saturation regime[41] after about 32 CO pulses and levels off at a value of ~115 ± 10 nJ per pulse at quasi-saturation. By dividing this measured energy input for any pulse by the absolute number of molecules in that pulse which adsorbed during the short-time sticking probability measurement, we obtain a heat of CO adsorption in kJ mol^{-1}, which is plotted as a function of CO surface coverage in Fig. 3e. On this surface, the heat of CO adsorption initially amounts to 125 kJ mol^{-1}. After adsorption of about 0.45×10^{15} CO molecules cm^{-2} the surface of the particles reaches the quasi saturation regime (with the corresponding CO surface coverage of ~0.5 ML with respect to the number of surface Pd atoms) and the adsorption heat levels out at ~77 kJ mol^{-1}. Note that no real coverage increase exists in the quasi steady state regime reached after about 8.5 s. Two reasons account for the decreasing adsorption enthalpy with growing CO coverage: intermolecular repulsion of neighboring CO molecules and increasing competition for the d-electrons of Pd nanoclusters participating in the CO–Pd bonding.

Qualitatively similar dependences of the sticking probabilities and the adsorption heat on the CO coverage were observed for all Pd particles and for the single crystal surface, which will be described in detail in Section 4.

4. CO adsorption energy and sticking probability as a function of particle size

As a next step, the dependence of the CO adsorption heat on the size of Pd nanoparticles was investigated for all five model catalysts and compared to the Pd(111) single crystal. As described above, the final energy value is the quotient of two independent measurements: the total amount of deposited energy and the number of adsorbed molecules associated with this energy transfer. The latter parameter was determined from the short-time sticking coefficient measurements of the King–Wells type[21] as described above. Fig. 4 shows, for all investigated model catalysts and the Pd(111) single crystal, the short-time sticking coefficients as a function of a number of adsorbed CO molecules (molecules cm^{-2}). In the following, we will denote the measured short-time sticking coefficient simply as a sticking coefficient.

All measurements were performed at 300 K, at which CO does not adsorb on the Fe_3O_4 support[23] but on the Pd particles only. Note that an apparent non-zero sticking coefficient was observed in the quasi steady state regime for all investigated surfaces, which arises from the partial CO desorption between the beam pulses and CO re-adsorption when the next pulse hits the surface (see discussion in Section 3). Fig. 5 displays the values of the *initial* sticking probability on the adsorbate-free Pd nanoparticles and on Pd(111) plotted as a function of the particle size (Fig. 5a) as well as the CO adsorption capacity (number of CO molecules adsorbed per cm^2 at saturation) reached right before the quasi steady state regime (Fig. 5b). This point at which the system reaches the quasi-steady state regime was chosen when the heat signal became constant (within its deviation of 4%) for all further CO pulses. Additionally we checked that the sticking coefficient values also remain constant (typically within ~5–10%). The first

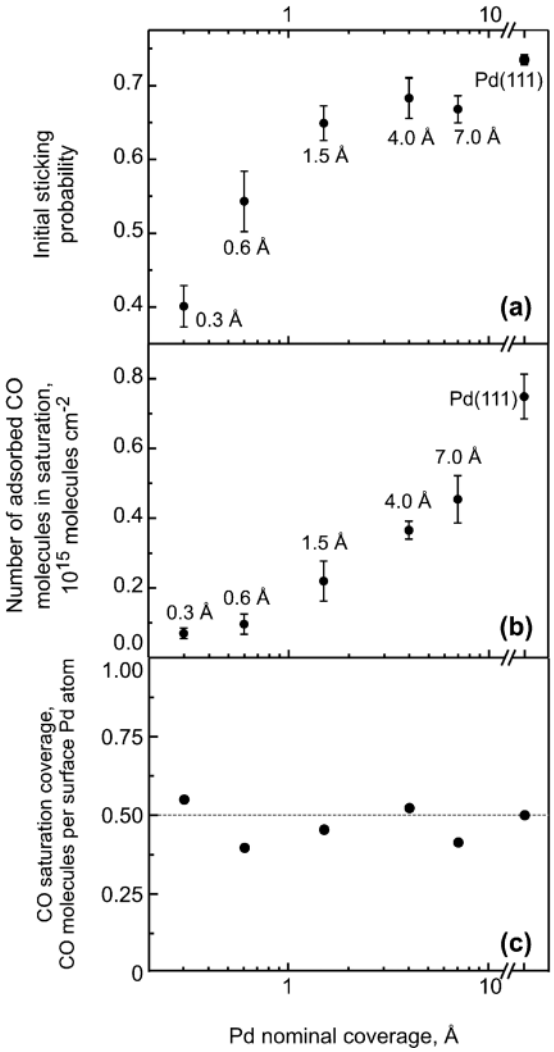

Fig. 5 Results of the sticking coefficient measurements on Pd(111) and Pd nanoparticles of different sizes plotted as a function of Pd nominal coverage: (a) initial sticking probability; (b) number of adsorbed CO molecules in quasi-saturation; (c) estimated CO saturation coverage expressed as a number of CO molecules per surface Pd atom. The error bars correspond to the error of the mean.

criterion was found to be more reliable, probably due to the better reproducibility of the heat measurement.

On Pd(111), the initial sticking probability reaches 0.72 ± 0.03 and remains nearly constant until the CO surface coverage of ~2.7 × 10^{14} CO molecules cm^{-2} (or 0.18 CO molecules per surface Pd atom) is achieved and decreases to a quasi steady state value of about 0.3 for a CO coverage of 0.76 × 10^{15} molecules cm^{-2} (or 0.5 CO molecules per surface Pd atom) in quasi saturation. The CO saturation coverage on Pd(111) is in an excellent agreement with the previously reported value, which was obtained by a number of independent surface-sensitive techniques (see *e.g.* ref. 42–45). The value of the initial sticking coefficient measured in this study is somewhat lower than the previously reported values 0.8–1.0[46] and 0.95 ± 0.05.[47]

It is apparent that the general adsorption mechanism follows a typical precursor type behavior, which was previously observed on the Pd single crystal surfaces (compare *e.g.* ref. 47). A similar precursor-mediated adsorption was detected for most of the Pd particle sizes except for the two smallest ones (0.3 and 0.6 Å deposition thickness). The CO adsorption capacity of the investigated surfaces increases with increasing particle size ranging from 0.07 × 10^{15} molecules cm^{-2} (for 0.3 Å Pd) to 0.45 × 10^{15} molecules cm^{-2} (for 7 Å). The CO surface coverage expressed as a number of adsorbed CO molecules per surface Pd atom is shown in Fig. 5c. Apparently, the CO surface coverage in saturation amounts to about 0.49 ± 0.06 CO molecules per surface Pd atom for all investigated particle sizes. This results in an excellent agreement with the CO saturation coverages of 0.5 measured on the Pd(111) and Pd(100) single crystal surfaces at room temperature (see *e.g.* ref. 42, 47 and 48). The largest deviation from the saturation coverage of 0.5 (by about 20%) was found for the deposition density of 0.6 Å, which can be related most likely to the error in the estimate of the number of Pd surface atoms. This result shows that the absolute adsorption capacity of all investigated Pd nanoparticles is close to the one of the single crystal surfaces and indicates that no dramatic changes in the adsorption mechanism occurs upon reduction of the particle sizes down to at least 2 nm.

The initial CO sticking probability on the Pd nanoparticles first linearly increases with increasing particles size (for the range of deposition thicknesses 0.3–1.5 Å) and then levels off at a constant value of ~0.67. These data are in very good experimental agreement with the previously obtained sticking coefficient data measured on Pd clusters in the same size range.[24]

The sticking coefficient data can be rationalized on a basis of the so-called "capture zone" effect, which was formulated for the supported catalysts by Matolin and Gillet.[49,50] This phenomenon is based on the existence of two adsorption channels: the adsorbate molecules can either directly impinge on the metal particles and chemisorb or they can be trapped in a weakly bound state on the support and reach the particles *via* surface diffusion. The capture zone was defined as an area from which impinging adsorbates can be collected by the particles. This effect was predicted and later experimentally confirmed to considerably enhance the adsorption rate on the particles [see *e.g.* ref. 11 and 51]. In the presented experiments, the capture zone effect was found to play an important role in the overall adsorption rate. The magnitude of this effect can be evaluated from the comparison of the measured initial sticking probability data on the supported particles and the estimate of the highest possible initial sticking probability on the particles of the same size in the absence of the contribution from the support. For the smallest deposition coverage of 0.3 Å, the average particle size of ~1.8 nm and the island density of 1.7 × 10^{12} particles per cm^2 result in the estimate that about 5% of the Fe_3O_4 surface area is covered by Pd particles. This means that only ~5% of the impinging molecules arrive directly on the metal surface and about 95% interact first with the support. If one assumes the highest possible sticking coefficient on metallic Pd to be 1.0 and fully neglects the contribution from the capture zone effect, only initial sticking coefficients below 0.05 can be expected (corresponding to the scenario when 5% of the molecules completely stick

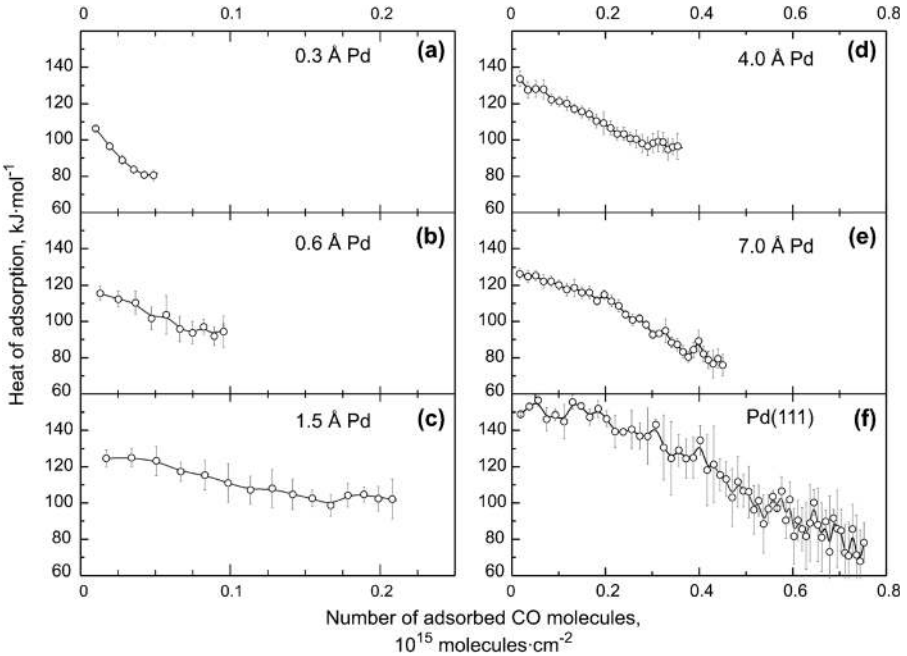

Fig. 6 Differential heats of adsorption plotted as a function of number of adsorbed CO molecules measured at 300 K for Pd(111) and for (a)–(e) Pd nanoparticles of different sizes (the Pd nominal coverages are indicated) and (f) for Pd(111). The data are shown as an average of four to six independent measurements on freshly prepared surfaces. The error bars correspond to the error of the mean.

to the metal particles). However, the experimentally measured initial sticking coefficient 0.4 is by an order of magnitude higher than the estimated upper limit for the direct sticking on the metal particles. This observation can be rationalized only in the scope of the "capture zone" model, where the additional 35% of the impinging molecules become first weakly trapped on the support and reach the Pd particles, where they strongly chemisorb, within their residence time. Thus, the capture zone effect leads to an enhancement of the adsorption rate by about a factor of 8. Note that CO does not chemisorb on Fe_3O_4 at the experimental temperature of 300 K [ref. 23 and this study], so that the enhanced adsorption cannot be explained simply by CO chemisorption on the support. Similar estimates can be made for the larger Pd particles. For the deposition thickness of 4 Å, about 48% of the total surface area is metallic, resulting in the upper limit for the direct sticking on Pd nanoparticles to be $\sim$0.48. The experimentally measured value of the initial sticking coefficient of 0.68 indicates that additionally 20% of the impinging molecules are trapped on the Fe_3O_4 support and diffuse to the particles within their residence time. A very similar result with the direct sticking coefficient on the particles of 0.50 and additional contribution from the support amounting to 0.17 was obtained for the large particles (7 Å nominal Pd coverage). It is apparent that the relative contribution from the trapping on the support decreases with increasing particle size: whereas the molecular flux from the support to the particles is by about a factor of 8 higher than the direct CO flux onto the nanoparticles for the smallest deposition coverage (0.3 Å), this ratio decreases to $\sim$0.4–0.35 for the two largest investigated particle sizes (4 and 7 Å, correspondingly). This effect can be explained most likely by the overlapping capture zones with increasing particle size, which reduces the relative fraction of the surface area contributing to the reverse spillover from the support to the metal.

The resulting differential adsorption heats plotted as a function of the number of adsorbed CO molecules are shown in Fig. 6 for all investigated particle sizes and Pd(111). Each curve is an average of 4 to 6 independent measurements on freshly prepared model systems. Qualitatively, the dependence of the adsorption heat on the adsorbate coverage is similar in all cases: after a high initial value, the adsorption heat decreases as a result of intermolecular repulsion between the adsorbates and increasing competition for Pd d-electrons participating in the CO–Pd bonding. Finally, the heat levels

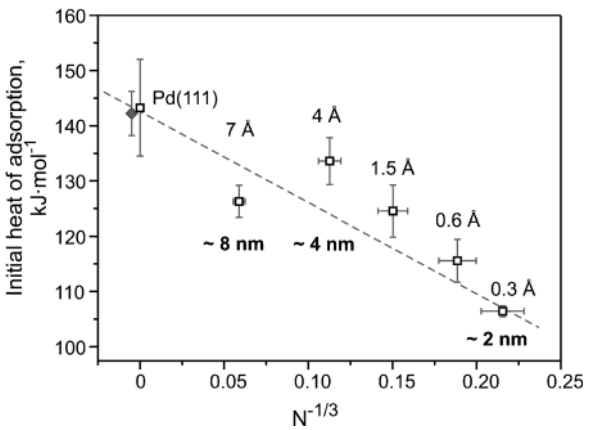

Fig. 7 Initial heats of adsorption as a function of $N^{-1/3}$, where N is the average number of atoms in a Pd particle (the Pd nominal coverage is indicated in the graph). $N^{1/3}$ is proportional to the effective diameter of a hemispherical particle. The filled diamond corresponds to the value of the CO adsorption heat on Pd(111) reported by Ertl *et al.*[46] Error bars correspond to the standard error of the mean.

off at a final non-zero value, which is associated with the dynamic adsorption–desorption equilibrium discussed in the Section 2. Note that the final heat value is a subject of large statistical errors since a very small absolute number of CO molecules is added in a single CO pulse that is difficult to measure.

The particle size dependence of the adsorption heat can be better analyzed by comparing the initial adsorption heats in the low coverage limit. Under these conditions, the adsorption heat is determined by the interaction of individual CO molecules with metal, and is not perturbed by the CO intermolecular repulsion or by the competition for the d-electrons. Fig. 7 shows the dependence of initial CO adsorption heats (measured during the first CO pulse) on the linear dimension of the particles expressed as $N^{-1/3}$, where N is the average number of Pd atoms per particle, which is proportional to the average particle volume. The Pd nominal coverage is indicated for each data point. The particles size dependence of the adsorption heats shows a pronounced trend: the initial heat of adsorption decreases with decreasing particle size, from 126 ± 3 kJ mol^{-1} on 8 nm-sized Pd particles to 106 ± 1 kJ mol^{-1} on the smallest ~1.8 nm clusters. Additionally, all investigated particles showed smaller initial adsorption heat as compared to the single crystal surface (149 ± 3 kJ mol^{-1}). Note that two experimental problems can principally affect the measured value of the initial adsorption heat. First, a variety of contaminating species such as water or CO adsorbed from the background prior to the microcalorimetric experiment can affect the measured initial heats of adsorption *e.g.* by selective blocking of the most stable adsorption sites. To check for possible contaminants and quantify their amounts, TPD experiments were performed for all prepared model supported systems and Pd(111) after a typical waiting time of 30 minutes between the cleaning at 600 K and the beginning of the calorimetric measurement. Neither water nor CO_2 traces were detected, and only negligible amounts of CO (~1% of the saturation coverage) were found to adsorb from the background after the cleaning of the sample. Second, different amounts of CO molecules per Pd particle could be adsorbed in the first pulse, giving rise to formally different CO coverages. Since the adsorption heat decreases due to inter-adsorbate repulsion, the heat values obtained at different CO coverages cannot be compared directly. To overcome this difficulty, we chose our experimental conditions in such a way that only a few molecules (0.01 to 0.06 CO molecules per surface Pd atom as estimated from the number of adsorbed molecules and the number of surface Pd atoms) are adsorbed after the first CO pulse (see Table 1 for more details). Therefore it can safely be assumed that the initial heats of adsorption were obtained in the low-coverage limit and governed predominantly by the interaction of a CO molecule with a Pd cluster and not by the repulsive interaction between the adsorbates.

The Pd particles investigated in this work expose mainly (111) terraces alongside with a smaller fraction of (100) facets and low-coordinated defect sites such as edges and corners. In the literature, there is a general agreement that the CO adsorption energy on the steps and open surfaces such as Pd(100) is only slightly higher than on the Pd(111) plane. Conrad and Ertl[46] studied the CO adsorption energies by equilibrium adsorption isotherm measurements on a variety of plane and stepped single crystal surfaces and found the lowest adsorption energy of about 142 kJ mol^{-1} for Pd(111), followed by the stepped surfaces (between 146 and 148.5 kJ mol^{-1}) and Pd(100) (153 kJ mol^{-1}). It appears to be difficult to compare these energies to the TPD data available from other groups because different assumptions on the pre-exponential factors were used. For the Pd(331) plane, Davies and Lambert[52] reported values between 143 and 150 kJ mol^{-1} depending on the chosen pre-exponential factors. This range lies somewhat higher than the value 142 kJ mol^{-1} reported by Conrad *et al.* for Pd(111). In agreement with Conrad and Ertl' study, Ramsier *et al.* found that the CO adsorption energy on the (100) plane is by about 10 to 15 kJ mol^{-1} higher than that on the (111) plane.[53] Theoretical calculations carried out by Yudanov *et al.* on Pd clusters in the size range of 55 to 260 Pd atoms per cluster agree well with the experimental data, showing that irregular sites *e.g.* edges exhibit higher CO adsorption energies than Pd(111).[54]

It should be noted, however, that the differences in the CO adsorption energies on the (111) facets and the low-coordinated sites (like step edges) are relatively small. Ramsier, Lee and Yates[53] even concluded from comparing CO TPD and adsorption energies for different stepped Pd facets that "structure of the Pd surface is only of minor importance in CO adsorption/desorption kinetics." These experimental results suggest that the degree of coordination of the Pd surface atoms on the stepped surfaces is not as important in determining the CO adsorption energy as on surfaces of other metals like Pt.[55] Even though the smaller particles exhibit larger relative amounts of low-coordinated Pd atoms, no major enhancement of the CO-binding energy can be expected due to increasing fraction of such sites. Instead, a pronounced decrease of the CO adsorption energy is experimentally observed for smaller particles, which has to be related to other size-dependent properties of Pd nanoclusters.

The observed decrease of the initial CO adsorption heat with decreasing particle size can be explained by two alternative microscopic effects: (i) reduction of the van der Waals attraction and (ii) weakening of the chemisorptive interaction.

First, a feasible weakening of the dispersion force (van der Waals interaction) that is induced by dynamic response of bulk electrons of the metal to charge density fluctuations in an adsorbed molecule can result in the decrease of adsorption heat of a gas-phase molecule on the small metal clusters. It has been previously shown that the electron population at the Fermi edge, which is mainly relevant for this interaction, drastically changes with the cluster size in the range of a few nanometres.[56] Since smaller clusters contain less electrons available for dynamic response, *i.e.* their polarizability is reduced, the decrease of the initial adsorption heat with the decreasing cluster size can be reasonably understood in the scope of this model. Similar behavior has been previously observed in TPD studies for methane on Pd[16] and NO on Ag nanoclusters[57] and was also attributed to the reduced polarizability of the small metal nanoparticles.

Second, the decrease of the chemisorption energy can arise from the lattice contraction of a small metal nanoparticle.

It is now well established by computational studies of various metals including Pd[58–60] that relaxed structures of metal clusters exhibit shorter interatomic distances than bulk crystals. Also experimental evidences for a pronounced decrease of the interatomic bond length with decreasing particle size are available from transmission electron microscopy (TEM) studies.[61,62] This phenomenon has been rationalized as a result of decreasing average coordination number of the atoms with the higher surface-to-volume ratio of the cluster.[58–60] Theoretical calculations on Pd clusters show that the average Pd–Pd nearest-neighbor distance decreases linearly with decreasing linear dimension of a nanoparticle in the range of 55–260 atoms per cluster.[63] This lattice contraction in the small metal clusters was theoretically shown to result in a reduction of the CO adsorbate binding energy. Particularly for the Pd clusters consisting of 55–260 atoms, which correspond to our smallest investigated cluster sizes, it was demonstrated that the clusters with the contracted lattice parameter exhibit systematically lower adsorption energies by about 10–15 kJ mol^{-1} than the clusters with a bulk terminated geometry (d(Pd–Pd) = 275 pm).[64] This finding can be rationalized in terms of the strain effect, which is associated with a downward shift of the valance d-band with decreasing lattice parameter[64,65] and results in a poorer overlap with the CO molecular orbitals. This effect also agrees with the principle of bond order conservation:[66,67] in the contracted clusters, one expects weaker adsorption bonds and stronger binding within the adsorbate as a result of better saturated valences of the substrate atoms. Theoretically, such effects were shown to be valid not only for 3-fold hollow sites on (111) facets, but also for the bridge and on-top sites and for the particle edges.[64] Thus, the effect of the lattice strain on the adsorption energy appears to reflect a general trend that holds for adsorption at any surface sites of the nanoparticles.

The relative contributions of the van der Waals interaction and chemisorption strength into overall reduction of the CO adsorption energy with decreasing particle size cannot be estimated from our experimental data. The large magnitude of the effect (about 40 kJ mol^{-1} relative to the Pd(111) surface) allows us to suggest that most likely reduction of both van der Waals interaction and chemisorption strength contributes to the overall decrease of the adsorption heat. To resolve this question, further theoretical calculations on clusters that treat both interactions are needed.

Conclusions

In conclusion, we investigated the interaction of CO molecules with well-defined Pd nanoclusters and with the extended Pd(111) surface under clean UHV conditions. The main focus of this study was the direct measurement of the CO adsorption heat by single crystal adsorption microcalorimetry and finding a correlation between the particle size and the gas–surface interaction strength. Pd particles of different average sizes ranging from 120 to 4900 atoms per particle (or from 1.8 to 8 nm) were used in this study, which were supported on a model *in situ* grown Fe_3O_4/Pt(111) oxide film.

To obtain reliable reflectivity values that are necessary for precise quantification of adsorption energies, the optical properties of the supported particles and the oxide film were investigated by a new *in situ* setup for reflectivity measurements. During the stepwise preparation of the Fe_3O_4 film, the reflectivity at a wavelength of λ = 632.8 nm was found to decrease linearly with increasing thickness of the oxide layer. A gradient of (0.19 ± 0.06)%/Å, where Å refers to the nominal iron coverage, was obtained. The optical reflectivity of the final oxide film, resulting from the total deposition of 24 Å of iron, was determined to be 69.2% at 298 K. The reflectivity for supported Pd particles of various sizes was found to lie in the range of 69 to 68% for average particle sizes from 1.8 to 8 nm (or nominal Pd deposition coverages 0.3 to 7 Å).

The CO adsorption kinetics investigated by the King–Wells method shows a strong enhancement due to a capture zone effect involving weak trapping of the adsorbates on the support and diffusion to the metal particles. This effect was quantified based on the structural data from STM. For the smallest particles containing 120 Pd atoms per particles, the CO adsorption rate was found to be enhanced by a factor of about 8. This factor decreases to $\sim$1.35–1.4 for the largest investigated particles.

The binding energy of carbon monoxide was found to considerably decrease with decreasing particle size. The obtained initial CO adsorption energy on the 1.8 nm-sized Pd clusters is reduced by about $\sim$20 kJ mol^{-1} as compared to the largest 8 nm particles and by $\sim$40 kJ mol^{-1} relative to the extended Pd(111) single crystal surface. With this we provided for the first time a direct experimental proof that the CO binding energy decreases with decreasing particle size and resolved a long-standing controversy. Two phenomena were suggested to contribute to the observed reduction of CO binding strength on the small nanoparticles: (i) reduction of van der Waals attraction due to the reduced polarizability of the small particles and (ii) weakening of chemisorptive interaction due to the contraction of the lattice parameter of the Pd cluster. The present data provide important benchmarks for upcoming theoretical calculation, incorporating dispersive van der Waals interactions.

Acknowledgements

The authors thank J.A. Farmer and J. Hartmann for technical support and valuable discussions. The work is supported by German Science Foundation (DFG), through collaborative research center 546 "transition metal aggregates" and through the Cluster of Excellence "Unifying concepts in catalysis" (UNICAT). We are also grateful to Fonds der Chemischen Industrie for financial support. SS acknowledges support from the Robert-Bosch-Stiftung (program "Fast Track"). CTC acknowledges the US DOE, OBES Chemical Sciences grant DE-FG02-96ER14630, for support of this work.

References

1 G. Ertl, H. Knoezinger and J. Weitkamp, in *Handbook of Heterogeneous Catalysis*, ed. G. Ertl, H. Knoezinger and J. Weitkamp, VCH, Weinheim, 1997.
2 A. T. Bell, *Science*, 2003, **299**, 1688.
3 M. Bäumer and H.-J. Freund, *Prog. Surf. Sci.*, 1999, **61**, 127.
4 C. T. Campbell, *Surf. Sci. Rep.*, 1997, **27**, 1.

5 M. Valden, X. Lai and D. W. Goodman, *Science*, 1998, **281**, 1647.
6 M. Haruta, *Catal. Today*, 1997, **36**, 153.
7 H.-J. Freund, *Surf. Sci.*, 2002, **500**, 271.
8 P. Chou and M. A. Vannice, *J. Catal.*, 1987, **104**, 1; B. Sen and M. A. Vannice, *J. Catal.*, 1991, **130**, 9; C. Leon and M. A. Vannice, *Appl. Catal.*, 1991, **69**, 269.
9 C. T. Campbell, A. W. Grant, D. E. Starr, S. C. Parker and V. A. Bondzie, *Top. Catal.*, 2000, **14**, 43.
10 H.-J. Freund, *Angew. Chem., Int. Ed. Engl.*, 1997, **36**, 452.
11 C. R. Henry, *Surf. Sci. Rep.*, 1998, **31**, 231.
12 D. R. Rainer and D. W. Goodman, *J. Mol. Catal. A: Chem.*, 1998, **131**, 259.
13 T. Schalow, B. Brandt, D. E. Starr, M. Laurin, S. K. Shaikhutdinov, S. Schauermann, J. Libuda and H.-J. Freund, *Angew. Chem., Int. Ed.*, 2006, **45**, 3693.
14 T. P. St. Clair and D. W. Goodman, *Top. Catal.*, 2000, **13**, 5.
15 I. Stará and V. Matolín, *Surf. Sci.*, 1994, **313**, 99.
16 K. Watanabe, Y. Matsumoto, M. Kampling, K. Al-Shamery and H.-J. Freund, *Angew. Chem., Int. Ed.*, 1999, **38**, 2192.
17 J.-H. Fischer, J. Hartmann, J. A. Farmer, J. M. Flores-Camacho, C. T. Campbell, S. Schauermann and H.-J. Freund, *Rev. Sci. Instrum.*, 2011, **82**, 024102.
18 T. Schalow, B. Brandt, M. Laurin, D. Starr, Sh. K. Shaikhutdivov, J. Libuda and H.-J. Freund, *Catal. Lett.*, 2006, **107**, 189.
19 C. Duriez, C. R. Henry and C. Chapon, *Surf. Sci.*, 1991, **253**, 190.
20 J.-H. Fischer-Wolfarth, J. A. Farmer, J. M. Flores-Camacho, A. Genest, I. V. Yudanov, N. Rösch, C. T. Campbell, S. Schauermann and H.-J. Freund, *Phys. Rev. B: Condens. Matter Mater. Phys.*, 2010, **81**, 241416(R).
21 D. King and M. Wells, *Surf. Sci.*, 1972, **29**, 454.
22 W. Weiss and W. Ranke, *Prog. Surf. Sci.*, 2002, **70**, 1.
23 C. Lemire, R. Meyer, V. Henrich, S. K. Shaikhutdinov and H.-J. Freund, *Surf. Sci.*, 2004, **572**, 103.
24 T. Schalow, B. Brandt, D. E. Starr, M. Laurin, S. K. Shaikhutdinov, S. Schauermann, J. Libuda and H.-J. Freund, *Phys. Chem. Chem. Phys.*, 2007, **9**, 1347.
25 T. Schalow, B. Brandt, M. Lurin, S. Schauermann, J. Libuda and H.-J. Freund, *J. Catal.*, 2006, **242**, 58.
26 C. Kittel, *Introduction to Solid State Physics*, John-Wiley & Sons, Inc, 8th edn, 2005.
27 A. Y.-C. Yu, W. E. Spicer and G. Hass, *Phys. Rev.*, 1968, **171**, 834.
28 A. Stuck, C. E. Wartnaby, Y. Y. Yeo, J. T. Stuckless, N. Alsarraf and D. A. King, *Surf. Sci.*, 1996, **349**, 229.
29 H. M. Ajo, H. Ihm, D. E. Moilanen and C. T. Campbell, *Rev. Sci. Instrum.*, 2004, **75**, 4471.
30 J. H. Weaver, *Phys. Rev. B: Solid State*, 1975, **11**, 1416.
31 A. Y.-C. Yu and W. E. Spicer, *Phys. Rev.*, 1968, **169**, 497.
32 P. B. Johnson and R. W. Christy, *Phys. Rev. B: Solid State*, 1974, **9**, 5056.
33 J. H. Weaver and R. L. Benbow, *Phys. Rev. B: Solid State*, 1975, **12**, 3509.
34 J. Lafait, F. Abeles, M. L. Theye and G. Vuye, *J. Phys. F: Met. Phys.*, 1978, **8**, 1597.
35 U. Kreibig and M. Vollmer, *Optical Properties of Metal Clusters*, vol. 25 of Springer Series in Materials Science, Springer-Verlag, Berlin, 1995.
36 C. F. Bohren and D. R. Huffman, *Absorption and scattering of light by small particles*, Wiley, New York, 1998.
37 J. Liu, M. Xu, T. Nordmeyer and F. Zaera, *J. Phys. Chem.*, 1995, **99**, 6167.
38 S. R. Longwitz, J. Schnadt, E. K. Vestergaard, R. T. Vang, E. Lægsgaard, I. Stensgaard, H. Brune and F. Besenbacher, *J. Phys. Chem. B*, 2004, **108**, 14497.
39 C. E. Borroni-Bird and D. A. King, *Rev. Sci. Instrum.*, 1991, **62**, 2177.
40 O. Lytken, W. Lew, J. Harris, E. Vestergaard, J. M. Gottfried and C. T. Campbell, *J. Am. Chem. Soc.*, 2008, **130**, 10247.
41 W. A. Brown, R. Kose and D. A. King, *Chem. Rev.*, 1998, **98**, 797.
42 A. M. Bradshaw and F. M. Hoffmann, *Surf. Sci.*, 1978, **72**, 513.
43 J. Szanyj, W. K. Kuhn and D. W. Goodman, *J. Vac. Sci. Technol., A*, 1993, **11**, 1969.
44 S. Surnev, M. Sock, M. G. Ramsey, F. P. Netzer, M. Wiklund, M. Borg and J. N. Andersen, *Surf. Sci.*, 2000, **470**, 171.
45 T. Gießel, O. Schaff, C. J. Hirschmugl, V. Fernandez, K.-M. Schindler, A. Theobald, S. Bao, R. Lindsay, W. Berndt, A. M. Bradshaw, C. Baddeley, A. F. Lee, R. M. Lambert and D. P. Woodruff, *Surf. Sci.*, 1998, **406**, 90.
46 H. Conrad, G. Ertl, J. Kocha and E. E. Latta, *Surf. Sci.*, 1974, **43**, 462.
47 T. Engel, *J. Chem. Phys.*, 1978, **69**, 373.
48 A. Ortega, F. M. Hoffmann and A. M. Bradshaw, *Surf. Sci.*, 1982, **119**, 79.
49 E. Gillet, S. Channakhone, V. Matolin and M. Gillet, *Surf. Sci.*, 1985, **152/153**, 603.
50 V. Matolin and E. Gillet, *Surf. Sci.*, 1986, **166**, 115.
51 J. Libuda and H.-J. Freund, *Surf. Sci. Rep.*, 2005, **57**, 157.
52 P. W. Davies and R. M. Lambert, *Surf. Sci.*, 1981, **111**, L671.
53 R. D. Ramsier, K.-W. Lee and J. T. Yates, Jr., *Surf. Sci.*, 1995, **322**, 243.
54 I. V. Yudanov, R. Sahnoun, K. M. Neyman, N. Rösch, J. Hoffmann, S. Schauermann, V. Johánek, H. Unterhalt, G. Rupprechter, J. Libuda and H.-J. Freund, *J. Phys. Chem. B*, 2003, **107**, 255.
55 C. T. Campbell, G. Ertl, H. Kuipers and J. Segner, *Surf. Sci.*, 1981, **107**, 207.
56 S. Sandel, J. Libuda, P. Brühwiler, S. Andersson, A. J. Maxwell, M. Bäumer, N. Mårtensson and H.-J. Freund, *J. Vac. Sci. Technol., A*, 1996, **14**, 1546.
57 D. Mulugeta, K. H. Kim, K. Watanabe, D. Menzel and H.-J. Freund, *Phys. Rev. Lett.*, 2008, **101**, 146103.
58 S. Krüger, S. Vent, F. Nörtermann, M. Staufer and N. Rösch, *J. Chem. Phys.*, 2001, **115**, 2082.
59 P. Nava, M. Sierka and R. Ahlrichs, *Phys. Chem. Chem. Phys.*, 2003, **5**, 3372.
60 O. Häberlen, S.-C. Chung, S. Krüger and N. Rösch, *J. Chem. Phys.*, 1997, **106**, 5189.
61 S. A. Nepijko, M. Klimenkov, M. Adelt, H. Kuhlenbeck, R. Schlögl and H.-J. Freund, *Langmuir*, 1999, **15**, 5309.
62 R. Lamber, S. Wetjen and N. I. Jaeger, *Phys. Rev. B: Condens. Matter*, 1995, **51**, 10986.
63 I. V. Yudanov, R. Sahnoun, K. M. Neyman and N. Rösch, *J. Chem. Phys.*, 2002, **117**, 9887.
64 I. V. Yudanov, M. Metzner, A. Genest and N. Rösch, *J. Phys. Chem. C*, 2008, **112**, 20269.
65 B. Hammer, Y. Morikawa and J. K. Nørskov, *Phys. Rev. Lett.*, 1996, **76**, 2141.
66 E. Shustorovich and H. Sellers, *Surf. Sci. Rep.*, 1998, **31**, 1.
67 R. A. van Santen and G. J. Kramer, *Chem. Rev.*, 1995, **95**, 637.

